

On the Reflectance of Uniform Slopes for Normally Incident Interfacial Solitary Waves

DANIEL BOURGAULT

Department of Physics and Physical Oceanography, Memorial University, St. John's, Newfoundland, Canada

DANIEL E. KELLEY

Department of Oceanography, Dalhousie University, Halifax, Nova Scotia, Canada

(Manuscript received 29 March 2005, in final form 2 September 2006)

ABSTRACT

The collision of interfacial solitary waves with sloping boundaries may provide an important energy source for mixing in coastal waters. Collision energetics have been studied in the laboratory for the idealized case of normal incidence upon uniform slopes. Before these results can be recast into an ocean parameterization, contradictory laboratory findings must be addressed, as must the possibility of a bias owing to laboratory sidewall effects. As a first step, the authors have revisited the laboratory results in the context of numerical simulations performed with a nonhydrostatic laterally averaged model. It is shown that the simulations and the laboratory measurements match closely, but only for simulations that incorporate sidewall friction. More laboratory measurements are called for, but in the meantime the numerical simulations done without sidewall friction suggest a tentative parameterization of the reflectance of interfacial solitary waves upon impact with uniform slopes.

1. Introduction

Diverse observational case studies suggest that the breaking of high-frequency interfacial solitary waves (ISWs) on sloping boundaries may be an important generator of vertical mixing in coastal waters (e.g., MacIntyre et al. 1999; Bourgault and Kelley 2003; Klymak and Moum 2003; Moum et al. 2003). Since mixing is important to many aspects of coastal ocean dynamics, these observations call for the development of a model capable of predicting ISW generation, propagation, and dissipation in hydrographically complex oceans and lakes. However, before such a generic model can be established, a number of specific problems related to ISW dynamics must be solved. In particular for this paper, the reflectance of shoaling boundaries for normally incident ISWs need to be better established.

The laboratory experiments of Helfrich (1992) and Michallet and Ivey (1999) provide the best available insight into this problem of slope reflectance. These

experiments addressed the idealized case of normally incident ISWs on uniform shoaling slopes in an otherwise motionless fluid with two-layer stratification. The results of these experiments showed that the fraction of ISW energy that gets reflected back to the source after impinging the sloping boundary depends on the ratio of the wavelength L_w and a length scale L_s characterizing the sloping boundary (see Fig. 1 for a definition sketch).

Unfortunately, from the point of view of extrapolation to the ocean, the reflectance values differ significantly between the experiments, as will be shown in section 3b. Helfrich (1992) reported reflectance values that were 0.1–0.4 lower than those of Michallet and Ivey (1999) for similar impinging waves. Since the reflectance is bounded between 0 and 1, these differences are large enough to merit further investigation.

To shed light on this issue, we have attempted to reinterpret the results of the laboratory experiment of Michallet and Ivey (1999). Our hypothesis is that sidewall friction might have introduced a bias in the analysis of the measurements. Noting the lack of theories that describe the shoaling, breaking, and reflectance of large-amplitude ISWs on steep slopes (see, e.g., the recent review of Ostrovsky and Stepanyants 2005; Helfrich and Melville 2006), we have addressed this prob-

Corresponding author address: Daniel Bourgault, Department of Physics and Physical Oceanography, Memorial University, St. John's, NL A1B 3X7, Canada.
E-mail: danielb@physics.mun.ca

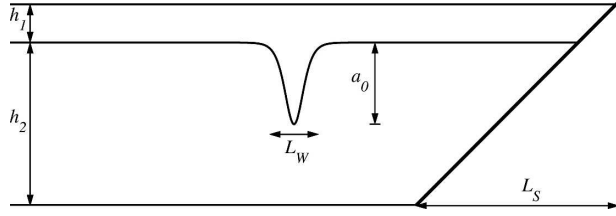


FIG. 1. Definition sketch showing an interfacial solitary wave of amplitude a_0 and length L_w [defined by Eq. (6) in the text], propagating in a two-layer fluid, with upper and lower undisturbed layer depths h_1 and h_2 (total depth $H = h_1 + h_2$), toward the sloping boundary of length L_s and slope $s = H/L_s$. This definition for L_s is from Michallet and Ivey (1999), and Helfrich (1992) defined L_s from the base of the slope to the interface–bottom intersection.

lem with a suite of fully nonlinear and nonhydrostatic two-dimensional numerical simulations. In these simulations the sidewall boundary condition is parameterized and is varied to mimic both laterally bounded laboratory domains and unbounded ocean domains.

The model we used and the simulations we carried out are described in the next section. After that, we outline the results and discuss their interpretation, highlighting the question of whether sidewall friction may have provided a bias in the laboratory results. We conclude with recommendations for future laboratory studies, and with a tentative parameterization.

2. Methods

a. General

The analysis makes use of a numerical model that integrates the laterally averaged Boussinesq Navier–Stokes equations. The model, described in detail by Bourgault and Kelley (2004), can simulate reasonably well the structure and velocity field of the first stages of a shoaling ISW when compared with the laboratory observation of Michallet and Ivey (1999). As shown in Bourgault and Kelley (2004), discrepancies between model results and laboratory observations become apparent during and after the transition to three-dimensional turbulence caused by the wave breaking on the slope. In the use of a two-dimensional model, we are thus working under the assumption that the reflection of normally incident waves does not depend on the three-dimensional stages of a shoaling wave event.

To address sidewall issues, we have incorporated a parameterization of sidewall friction by analogy to common bottom-friction parameterizations used in shallow water models. The laterally averaged drag force per unit mass is represented as

$$\mathbf{F}_s = \frac{\tau_s|_{y=B} - \tau_s|_{y=0}}{\rho_0 B}, \quad (1)$$

where y is the across-tank spatial coordinate, B is the tank width, ρ_0 is a reference density, and $\tau_s|_{y=B}$ and $\tau_s|_{y=0}$ are the stresses at the sidewalls. These stresses are parameterized following boundary layer theory (Kundu 1990, p. 312) as

$$\tau_s|_{y=B} = -\frac{1}{2}\rho_0 C_D |\mathbf{u}| \mathbf{u} \quad \text{and} \quad \tau_s|_{y=0} = \frac{1}{2}\rho_0 C_D |\mathbf{u}| \mathbf{u}, \quad (2)$$

where \mathbf{u} is the two-dimensional velocity field (i.e., along tank and vertical) and C_D is a drag coefficient whose value was tuned in the simulations to test sensitivity to sidewall drag. Inserting Eq. (2) into Eq. (1) gives

$$\mathbf{F}_s = -C_D \frac{|\mathbf{u}| \mathbf{u}}{B}. \quad (3)$$

b. Simulations of laboratory experiments

Simulations were performed with geometries and control parameters matching the experiments of Michallet and Ivey (1999). In these experiments measurements were made of the reflectance defined as

$$R = E_R/E_0, \quad (4)$$

where E_0 is the total energy of the incoming ISW measured at the base of the slope and E_R is the energy of the wave that is reflected back from the sloping bottom, also measured at the base of the slope.

Michallet and Ivey (1999) related the reflectance to the length ratio L_w/L_s (Fig. 1). More recently, Boegman et al. (2005) have argued that this parameter is not suitable for generalizing the laboratory results to field-scale situations because it is independent of the boundary slope. These authors have proposed the use of the Iribarren number, defined as

$$\xi = s/(a_0/L_w)^{1/2}, \quad (5)$$

where s is the slope of the linear topography and a_0 is the wave amplitude (see Fig. 1). We will adopt the Boegman et al. (2005) recommendation and present our results as a function of ξ instead of L_w/L_s .

Thirty-three numerical simulations were carried out (Table 1). From each run the values of a_0 , L_w , E_0 , and E_R were extracted, as explained in the following paragraphs, and were compared with the laboratory measurements of Michallet and Ivey (1999). All simulations were carried out on a grid of horizontal and vertical spacing $\Delta x = 2.5$ mm and $\Delta z = 1.25$ mm, of maximum depth $H = 15$ cm and of constant width $B = 25$ cm. The model is thus configured in a large-eddy mode, with a grid fine enough to resolve the ISW breaking and some of the collapse into smaller scales, but not the dissipa-

TABLE 1. Summary of numerical simulations. The densities of the top and bottom layers are ρ_1 and ρ_2 respectively. The experiment identifiers 1–16 match the identifiers used by Michallet and Ivey (1999, their Table 1), and the control parameters are set to match these laboratory experiments. The identifiers a and b refer to two different types of sidewall boundary conditions. In suite a, free-slip sidewalls are used; in suite b, no-slip sidewalls are used with $C_D = 0.2$ as inferred by calibrating the model to laboratory measurements (see section 3a).

No.	ρ_1/ρ_2	$h_2/(h_1 + h_2)$	L_s (cm)	s
1 b	1.039	0.66	0	∞
2 a, b	1.040	0.82	0	∞
3 a, b	1.020	0.65	217	0.069
4 a, b	1.020	0.78	217	0.069
5 a, b	1.040	0.70	217	0.069
6 a, b	1.039	0.90	217	0.069
7 a, b	1.040	0.67	89	0.169
8 a, b	1.040	0.83	89	0.169
9 a, b	1.040	0.91	89	0.169
10 a, b	1.013	0.63	70	0.214
11 a, b	1.013	0.71	70	0.214
12 a, b	1.012	0.84	70	0.214
13 a, b	1.044	0.60	70	0.214
14 a, b	1.046	0.67	70	0.214
15 a, b	1.047	0.77	70	0.214
16 a, b	1.048	0.80	70	0.214

tive scale (of order 0.1 mm). The model domain is closed on all sides, except at the free surface. The viscosity and diffusivity are set to the constant values $\nu = 10^{-6} \text{ m}^2 \text{ s}^{-1}$ and $\kappa = 10^{-7} \text{ m}^2 \text{ s}^{-1}$. A no-slip bottom- and end-wall boundary condition was used in all simulations.

To shed light on the issue of sidewall friction, two combinations of side boundary conditions were examined. The sequence of runs denoted “a” used free-slip sides (i.e., $C_D = 0$), and runs “b” used no-slip sides (i.e., $C_D > 0$).

Figure 2 shows the model geometry and the initial density field used in run 8a to generate a shoreward-propagating ISW partly reflecting and breaking against the sloping boundary. Run 8 is chosen as a typical example of results obtained for an intermediate value of $\xi \approx 0.6$ within the range examined (i.e., $0.2 \leq \xi \leq 1.7$).

As defined in Michallet and Ivey (1999), the characteristic ISW length scale was computed using

$$L_w = \frac{1}{a_0} \int_{x_1}^{x_2} |\eta(x)| dx, \quad (6)$$

where η is the interface displacement and x_1 and x_2 are taken by visual inspection to include the entire wave. For example, for the case shown in Fig. 2 (middle panel) the integration was between $x_1 = 50$ cm and $x_2 = 150$ cm. Choosing instead $x_1 = 25$ cm and $x_2 = 175$ cm suggests an uncertainty of $\pm 1\%$ for L_w .

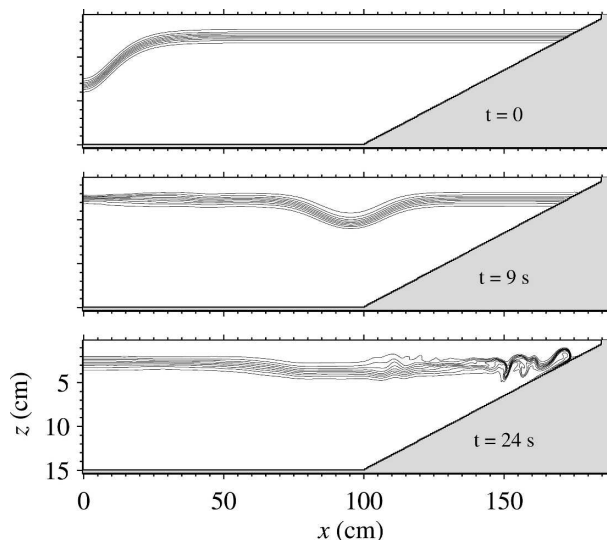


FIG. 2. (top) Model geometry and initial density field used in experiment 8a (see Table 1) to generate (middle) an internal solitary wave (bottom) reflecting and breaking onto a uniform shoaling slope.

The wave energies E_0 and E_R were calculated as a time integral of the depth-integrated energy flux F at the base of the slope, that is, with

$$E_0 = \int_{t_1}^{t_2} F dt \quad \text{and} \quad E_R = \left| \int_{t_3}^{t_4} F dt \right|, \quad (7)$$

where the intervals $[t_1, t_2]$ and $[t_3, t_4]$ are chosen visually to include the entire wave period, as illustrated below. Similar to Helfrich (1992), the depth-integrated energy flux is calculated as

$$F = \int_0^H u[p' + \rho_0(u^2 + w^2)] dz, \quad (8)$$

where p' is the wave-induced pressure (i.e., the instantaneous pressure minus the pressure in the undisturbed state), and u and w are horizontal and vertical velocity components. Note that in calculating wave energies Michallet and Ivey (1999) neglected the contribution of the terms in Eq. (8) that are nonlinear in velocity. Over the range of parameters examined, the neglect of those terms yields changes in reflectance R that are small relative to experimental errors.

Figure 3 shows the time series for F for experiment 8a. The peak centered around $t = 9.5$ s is the energy flux of the incoming wave. The trough centered around $t = 23$ s is the reflected wave energy flux. The second peak and trough centered around $t = 43$ s and $t = 60$ s respectively represent the second shoaling due to wave reflection at the generation side, which is disregarded in

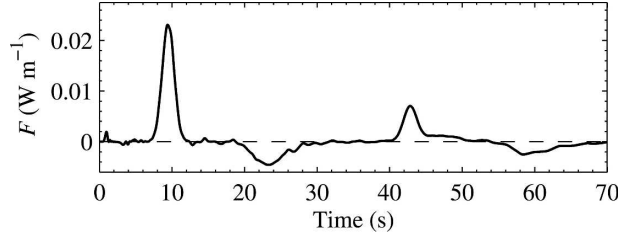


FIG. 3. Time series of the depth-integrated wave energy flux F computed at the base of the slope ($x = 100$ cm) for experiment 8a of Table 1 and Fig. 2.

the following analysis. For this case E_0 was computed by integrating F from $t_1 = 5 \pm 2$ s to $t_2 = 15 \pm 2$ s and E_R from $t_3 = 17 \pm 2$ s to $t_4 = 38 \pm 2$ s. The error associated with the integration limits leads to an uncertainty in E_R/E_0 of $\pm 5\%$.

3. Results

a. Viscous damping and sidewall friction

Michallet and Ivey (1999) estimated the energy dissipation of ISWs propagating at constant depth in their experiment (see their Fig. 7). Their laboratory measurements are reproduced in Fig. 4, which shows the instantaneous wave energy E relative to the initial wave energy E_i , as a function of the normalized traveled distance, that is, $x/H(h_2/H)^2$ [note that the waves were free to reflect at each end of the tank and that one flume length corresponds to $x/H(h_2/H)^2 \approx 10$]. The average energy lost across one flume length is roughly 0.01 J m^{-2} .

Figure 4 also shows the wave energy lost in the model during the propagation of an ISW in a channel of constant depth using free-slip sidewalls (run 2a in Table 1). In this model setup, the energy loss is caused by bottom friction and interfacial shear. The wave energy lost in the model during wave propagation over the length of one flume is roughly 10 times less than in the laboratory. Since the model has been set up to mimic the laboratory scales, we infer that there must be a dissipative mechanism in the laboratory that is not included in this model configuration.

One possibility is that turbulent dissipation occurs during wave propagation at the interfacial sheared layer, a process that would be incorrectly simulated with our two-dimensional model. However, this is judged to be unlikely, given that Michallet and Ivey (1999) observed the waves to be laminar during propagation without developing shear instabilities. The same comment can be made regarding our simulated waves during propagation: the waves always remained laminar. This suggests that interfacial shear-induced turbu-

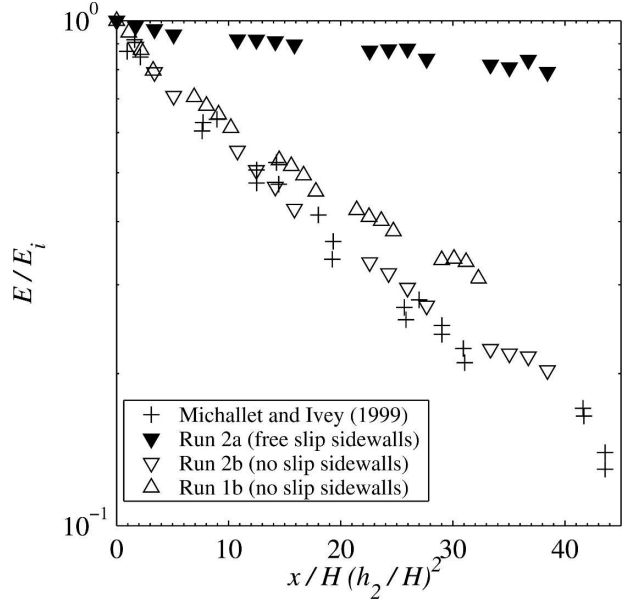


FIG. 4. Decrease of wave energy (E/E_i) against the normalized traveled distance $x/H(h_2/H)^2$ for waves propagating at constant depth.

lence is not the source of the energy loss during propagation in these experiments.

Another possibility is that wave energy is dissipated by the sidewall drag of the tank in addition to the dissipation arising from the bottom boundary layer. This effect can be parameterized with a sidewall drag coefficient, C_D , as in Eq. (3).

As a guide for the choice of the value of C_D , we note that since the bottom and sidewalls of the tank are made of the same material, the bottom and sidewall boundary layers should be comparable. Figure 5 shows the horizontal velocity structure u for the wave of experiment 2a along with the bottom shear stress

$$\tau_b = \rho_0 \nu \left. \frac{\partial u}{\partial z} \right|_{z=H}, \quad (9)$$

which is resolved by the model without the need for a drag formulation. The bottom boundary layer is roughly 1 cm thick and is characterized by flow separation at $x = 158$ cm caused by the current deceleration in the back of the wave. This flow separation is also depicted in the bottom shear stress τ_b being negative for $x < 158$ cm. The existence of flow separation is expected to add an additional form drag to the skin friction drag (Kundu 1990).

Using (2) we can estimate the bottom skin friction drag coefficient for $x > 158$ cm as

$$C_D^b = 2 \frac{\tau_b}{\rho_0 U^2}, \quad (10)$$

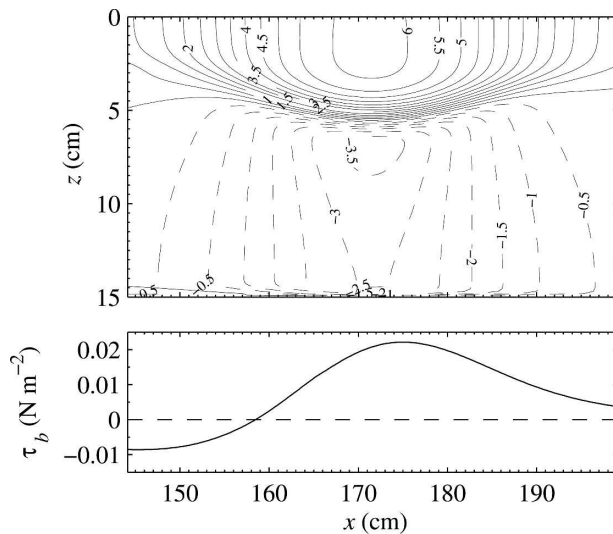


FIG. 5. (top) Horizontal velocity u (cm s^{-1}) and (bottom) bottom shear stress τ_b induced during wave propagation at constant depth (experiment 2a).

where U is the horizontal velocity just outside the boundary layer. For instance at $x = 175$ cm the stress has a maximum value of $\tau_b \approx 0.01 \text{ N m}^{-2}$ and the current above the boundary layer is $U \approx 0.03 \text{ m s}^{-1}$. Using $\rho_0 = 1040 \text{ kg m}^{-3}$, we get $C_D^b \approx 0.04$. Near the front of the wave at $x = 195$ cm, $U \approx 0.005 \text{ m s}^{-1}$, and $\tau_b = 0.005 \text{ N m}^{-2}$ giving $C_D^b \approx 0.4$. Averaged over the length of the wave, the bottom boundary layer is characterized by a drag coefficient of $O(0.1)$. We thus expect the sidewalls drag coefficient C_D to be of the same order of magnitude.

To test this, we adjusted the sidewall drag coefficient C_D in Eq. (3) to minimize the discrepancy between propagation losses in the laboratory and in the numerical simulations. This calibration yielded the value $C_D = 0.2$ (Fig. 4).

To validate this choice of sidewall friction coefficient we carried out another simulation with a dynamically different wave characterized by the parameters of experiment 1. The value of $C_D = 0.2$ yielded a decrease rate comparable to the previous case for $x/H(h_2/H)^2 \leq 10$ (Fig. 4). The fit with the laboratory measurements for these two cases suggests that sidewall friction is appropriately parameterized with Eq. (2) using $C_D = 0.2$.

b. Reflectance

Figure 6 shows the dependence of reflectance R on Iribarren number ξ for the two sets of numerical simulations (a and b) and for the laboratory measurements of Michallet and Ivey (1999).

For both sets of simulations (a and b) the results

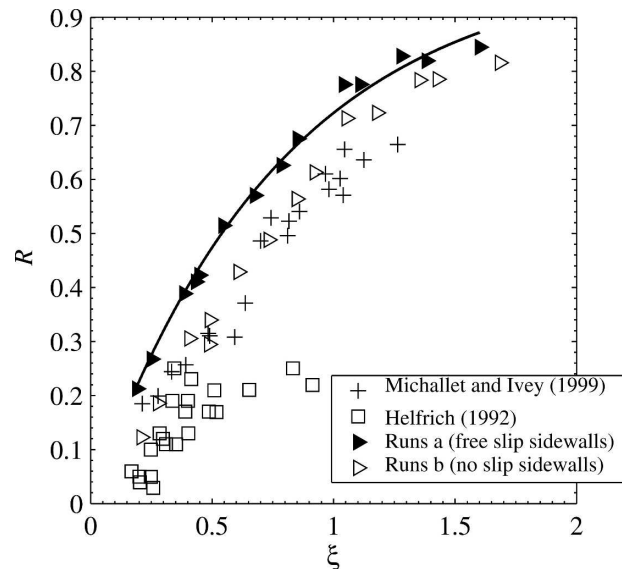


FIG. 6. Dependence of reflection coefficient R defined by Eq. (4) on the Iribarren slope parameter ξ defined in Eq. (5). The solid line is the exponential fit to case b given by Eq. (11).

display a trend that is similar to that of the measurements of Michallet and Ivey (1999). The fit is best for the simulations in which sidewall friction is included. For these cases, the simulated reflectance falls within the uncertainty of the laboratory measurements. However, for application to ocean and lake cases in which sidewall effects are not important, the most relevant simulations are those with free-slip sidewalls. The reflectance is approximately 0.1 larger in these simulations.

For comparison, the Helfrich (1992) measurements of reflectance, which we digitized from his Fig. 15, are also plotted in Fig. 6. Note that Helfrich (1992) presented his measurements as a function of a different length scale ratio than Michallet and Ivey (1999). Care must thus be taken in reporting his reflectance values in terms of the Iribarren number. Helfrich (1992) provides all the necessary information to do the conversion. Helfrich (1992) reflectance values are systematically smaller by 0.1–0.4 than those of Michallet and Ivey (1999). The reason for this disagreement is unclear. A possible explanation is that the Helfrich (1992) measurements were also influenced by sidewall friction but to a different extent since he used a different tank geometry and experimented with longer- and smaller-amplitude waves than Michallet and Ivey (1999). Consequently, the reflection coefficients of Helfrich (1992) may not be directly compared with those of Michallet and Ivey (1999), unless sidewall friction effects could be removed from both experiments.

As a guide to the eye, and as a tentative parameter-

ization, we performed a curve fit to the model results in which sidewall friction is neglected. Lacking a theoretical foundation for the dependency of R on ξ , a saturating-exponential functional form

$$R = 1 - e^{-\xi/\xi_0} \quad (11)$$

was used. A least squares fit with bootstrapped confidence intervals (CI) yields $\xi_0 = 0.78 \pm 0.02$ (95% CI) with root-mean-square deviation 0.02.

4. Discussion

The present numerical results suggest that sidewall friction was a significant factor in the laboratory experiments of Michallet and Ivey (1999). This is true even though the measurements were made at the base of the slope, in an attempt to minimize sidewall effects during propagation over the main part of the tank. Our results suggest that dissipation was occurring along the sidewalls as the wave propagated from the base of the slope, where the characteristics were measured, to the reflection site. Similarly, the reflected waves must also dissipate energy while propagating from the reflection site to the base of the slope, where their characteristics are also measured. This reasoning implies that E_0 in the denominator of Eq. (4) is overestimated as compared with the actual wave energy that reaches the reflection site, and that E_R is underestimated as compared with the actual energy that gets reflected. Taken together, these effects suggest that the reflectance is underestimated in the Michallet and Ivey (1999) experiments.

This result is reminiscent of the flat-bottom laboratory study of small-amplitude interfacial waves by Troy and Koseff (2006). These authors found sidewall friction to be the dominant wave-damping mechanism, provided that the nondimensional tank width B/h is less than 3, where h is either the upper- or lower-layer thickness. Direct comparison of these experiments is not possible because the wave amplitudes were small and the layers were of equal thickness. However, we note that on average, the Michallet and Ivey (1999) experiments are characterized with $B/h_1 \sim 6$ and $B/h_2 \sim 2$. Assuming that the Troy and Koseff (2006) criterion holds roughly for the large-amplitude waves considered here, the dissipation in the bottom layer is dominated by sidewall friction.

If sidewall effects are important for calculating the reflectance R , as we are suggesting, this will have repercussions on other quantities related to the mixing properties of shoaling boundaries. For example, a quantity of particular interest is the mixing efficiency defined by Michallet and Ivey (1999) as

$$\Gamma_{\text{MI}} = \frac{\Delta P}{E_0 - E_R} = \frac{\Delta P}{E_0} \frac{1}{(1 - R)}, \quad (12)$$

where ΔP is the increase in the irreversible potential energy caused by wave breaking on the slope. Thus, errors in R lead to errors in Γ_{MI} . Note that in a similar experiment Helfrich (1992) took into account sidewall friction in calculating mixing efficiency. Using an extended version of the Korteweg–de Vries equation that took into account variable depth and sidewall friction, he estimated the fraction α of the wave energy at the base of the slope E_0 that remained at the breaking point. In contrast to Michallet and Ivey (1999), Helfrich (1992) defined mixing efficiency as

$$\Gamma_{\text{H}} = \frac{\Delta P}{\alpha E_0 - E_R} = \frac{\Delta P}{E_0} \frac{1}{(\alpha - R)}, \quad (13)$$

with $0.7 < \alpha < 0.9$.

The present analysis supports the use of a formulation like Eq. (13) for minimizing biases associated with the loss of energy in the slope region caused by sidewall friction. To be more general, we could argue that a factor $\alpha/R > \beta > 1$ should be incorporated as in

$$\Gamma = \frac{\Delta P}{\alpha E_0 - \beta E_R} = \frac{\Delta P}{E_0} \frac{1}{(\alpha - \beta R)}, \quad (14)$$

in order to correct for the energy loss while the reflected wave propagates from the reflection site to the base of the slope, where its energy is evaluated. Another option to reduce the bias would be to use a tank large enough so that sidewall friction could be neglected, as suggested by Troy and Koseff (2006).

5. Conclusions

Our numerical simulations suggest that Michallet and Ivey (1999) underestimated the reflectance of uniform slopes for normally incident interfacial solitary waves, owing to a neglect of sidewall frictional effects. However, the fact that our two-dimensional model does not explicitly resolve sidewall boundary layers prevents us from making firm conclusions on this issue. More laboratory measurements or three-dimensional numerical simulations are needed. However, in the meantime, Eq. (11) provides a tentative parameterization for the reflectance of smooth uniform slopes on normally incident and laminar interfacial solitary waves without sidewall effects.

Acknowledgments. We thank Ramzi Mirshak and the anonymous reviewers for their insightful comments. This work was supported by the Natural Sciences and Engineering Research Council of Canada and by the Canadian Foundation for Climate and Atmospheric Sciences.

REFERENCES

- Boegman, L., G. N. Ivey, and J. Imberger, 2005: The degeneration of internal waves in lakes with sloping topography. *Limnol. Oceanogr.*, **50**, 1620–1637.
- Bourgault, D., and D. E. Kelley, 2003: Wave-induced boundary mixing in a partially mixed estuary. *J. Mar. Res.*, **61**, 553–576.
- , and —, 2004: A laterally averaged nonhydrostatic ocean model. *J. Atmos. Oceanic Technol.*, **21**, 1910–1924.
- Helfrich, K. R., 1992: Internal solitary wave breaking and run-up on a uniform slope. *J. Fluid Mech.*, **243**, 133–154.
- , and W. K. Melville, 2006: Long nonlinear internal waves. *Annu. Rev. Fluid Mech.*, **38**, 395–425.
- Klymak, J. M., and J. N. Moum, 2003: Internal solitary waves of elevation advancing on a shoaling shelf. *Geophys. Res. Lett.*, **30**, 2045, doi:10.1029/2003GL017706.
- Kundu, P. K., 1990: *Fluid Mechanics*. Academic Press, 638 pp.
- MacIntyre, S., K. M. Flynn, R. Jellison, and J. Romero, 1999: Boundary mixing and nutrient fluxes in Mono Lake, California. *Limnol. Oceanogr.*, **44**, 512–529.
- Michallet, H., and G. N. Ivey, 1999: Experiments on mixing due to internal solitary waves breaking on uniform slopes. *J. Geophys. Res.*, **104**, 13 467–13 477.
- Moum, J. N., D. M. Farmer, W. D. Smyth, L. Armi, and S. Vagle, 2003: Structure and generation of turbulence at interfaces strained by internal solitary waves propagating shoreward over the continental shelf. *J. Phys. Oceanogr.*, **33**, 2093–2112.
- Ostrovsky, L. A., and Y. A. Stepanyants, 2005: Internal solitons in laboratory experiments: Comparison with theoretical models. *Chaos*, **15**, 037111, doi:10.1063/1.2107087.
- Troy, C. D., and J. R. Koseff, 2006: The viscous decay of progressive interfacial waves. *Phys. Fluids*, **18**, 026602, doi:10.1063/1.2166849.